Inhomogeneous NMR line shape as a probe of microscopic organization of bicontinuous cubic phases

ARTICLE *in* THE JOURNAL OF PHYSICAL CHEMISTRY B · MAY 2008

Impact Factor: 3.3

4 AUTHORS:

Konstantin Momot
Queensland University of Technology
39 PUBLICATIONS **413** CITATIONS
SEE PROFILE

Kiyonori Takegoshi
Kyoto University
170 PUBLICATIONS **3,045** CITATIONS
SEE PROFILE

Philip W Kuchel
University of Sydney
308 PUBLICATIONS **5,153** CITATIONS
SEE PROFILE

Timothy J Larkin
University of Cambridge
35 PUBLICATIONS **64** CITATIONS
SEE PROFILE

Inhomogeneous NMR Line Shape as a Probe of Microscopic Organization of Bicontinuous Cubic Phases

Konstantin I. Momot,*,† K. Takegoshi,‡ Philip W. Kuchel,§ and Timothy J. Larkin§

School of Physical and Chemical Sciences, Queensland University of Technology, GPO Box 2434, Brisbane, Qld 4001, Australia, Department of Chemistry, Kyoto University, Kyoto, Japan, and School of Molecular and Microbial Biosciences, University of Sydney, Sydney, NSW 2006, Australia

Received: January 22, 2008; Revised Manuscript Received: February 27, 2008

NMR line shapes of the lipid and aqueous species in bicontinuous cubic phase (BCP) samples prepared by centrifugation are inhomogeneously broadened. The broadening of the lipid peaks is removed by magic-angle spinning (MAS). In this work, we studied the mechanism of this broadening using ^{1}H and ^{13}C NMR spectroscopy of a myverol/water BCP. It is demonstrated that the inhomogeneity possesses an intrinsic contribution that is independent of instrumental or setup factors and can be attributed to the microscopic organization of the BCP bilayer. A mechanism of the inhomogeneous broadening is proposed, which involves a spatially nonuniform diamagnetically induced magnetic field determined by the mesoscopic structure and the diamagnetic susceptibilities of the two BCP domains. The proposed mechanism does not require that molecular reorientation of the lipid be slow for the inhomogeneous broadening to survive. We discuss how this inhomogeneous broadening can be employed as a probe of compositional uniformity and microscopic organization of BCP samples.

Introduction

BCP are thermodynamically stable lipid/water liquid crystalline systems characterized by a mesoscopic periodic structure possessing medium- to long-range cubic periodicity.[1,2] In the static limit, the geometry of the lipid bilayer can be approximated by an infinite periodic minimal surface (IPMS); two congruent but nonintersecting channel systems are occupied by aqueous medium. A schematic diagram of a BCP of the *Ia*3*d* spatial symmetry is shown in Figure 1. BCPs have found uses in controlled-release drug delivery[3–7] and crystallization of membrane proteins[8,9] and have provided an interesting in vitro model for studying the effects of curvature on the properties of the lipid bilayer.[10,11] These applications have presented the need for the understanding of functional properties and rational design of BCP-based and similar materials, motivating studies of their microstructure and molecular mobility.[12–18]

NMR lines of the lipid and aqueous species in BCP samples are inhomogeneously broadened.[19] Several potential causes of this broadening have been proposed. MAS has been shown to reduce or eliminate the broadening, resulting in improved NMR spectral resolution as compared to the static samples.[19] MAS diffusion measurements of related lyotropic systems have also provided insights into the diffusional behavior of the lipid.[20] Recently, a new line-narrowing technique, consisting of loading BCP samples into thin-walled glass capillaries, has been discovered.[21] In this work, we focus on investigating the mechanism of the inhomogeneous broadening in BCP samples. This is done with a view to using NMR line shape inhomogeneity as a probe of the microscopic organization of BCPs, as has previously been done in other materials.[22–25] We present a number of observations demonstrating the intrinsic nature of the inhomogeneous line broadening in BCPs, most importantly, the differential MAS line narrowing between the water and the lipid species.

We used the myverol/H_2O system, which is well-characterized and forms an *Ia*3*d* BCP above 23 °C near the composition point 70% lipid:30% H_2O (w/w).[26] Nonspinning ^{1}H NMR spectra of this system exhibited distinctly inhomogeneous line shapes. We demonstrate that at least some of this inhomogeneous broadening is independent of the experimental setup and conditions and is intrinsic to the lyotropic lipid/water cubic phase. We discuss a number of candidate mechanisms of the line broadening observed and propose one in which the survival of the inhomogeneous broadening does not require molecular reorientation to be slow. This mechanism involves a nonuniform-induced magnetic field in a system consisting of two domains with different diamagnetic susceptibilities ("lipid" and "water"). The proposed mechanism is supported by the results of numerical simulations of the induced magnetic field in model lipid/water systems.

Methods

Sample Preparation. BCP samples were prepared from water and myverol (CAS 85586-30-7). Myverol is a mixture of monoacylglycerol lipids, in which 1-monoolein (CAS 25496-72-4) is the major component. It is frequently used as an inexpensive alternative to monoolein because of the similarity of their lipid/water phase diagrams.[26] Three BCP samples were examined as follows: sample **1**, myverol:H_2O 70:30%; sample **2**, 75.9:24.1%; and sample **3**, 75.2:24.8% (all w/w). Cubic phase samples were prepared by combining the required quantities of lipid and saline in a centrifuge tube. The samples were homogenized by repeated cycles of centrifugation at 12000*g*, manual stirring, and incubation at 25 °C over a period of 2−3 days. Following preparation, the samples were stored at 25 °C to avoid the coexistence of the lamellar crystalline phase (L_c).[26] NMR measurements were performed within 3 days of sample preparation. The chemicals used were obtained from the following sources: Myverol 18-99 was from Quest International

* To whom correspondence should be addressed. Fax: +61 7 3138 1521. E-mail: k.momot@qut.edu.au.
† Queensland University of Technology.
‡ Kyoto University.
§ University of Sydney.

10.1021/jp8006415 CCC: $40.75
Published on Web 05/06/2008

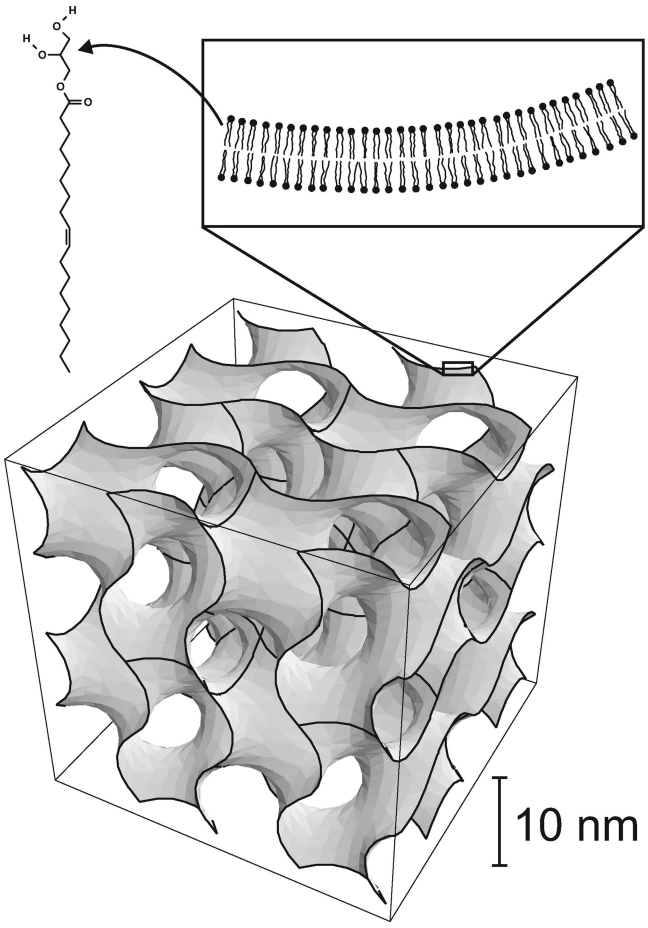

Figure 1. Schematic drawing of the Ia3d BCP. The average center of the bilayer follows the gyroid minimal surface.

(Zwijndrecht, The Netherlands); PBS (osmolality, 265 ± 1 mmol kg^{-1}; 0.01 M phosphate buffer, 0.0027 M KCl, and 0.137 M NaCl, pH 7.4, at 25 °C) was prepared from PBS concentrate (Sigma-Aldrich, United States). Myverol was dried by rotary evaporation at 52 °C followed by freeze drying and was stored under argon.[16] Other reagents were used as received.

High-Resolution Solution Spectra. Spectra of myverol solutions in CD_3OD were recorded at $B_0 = 9.4$ T using a Bruker DRX-400 NMR spectrometer equipped with a 5 mm TXI probe. The spectrometer has been described previously,[27,28] and standard NMR procedures were used. The spectra were recorded from static 5 mm samples.

Static BCP Spectra. BCP samples **1** and **2** were loaded either in a 5 mm Shigemi NMR tube susceptibility-matched to D_2O or in a 8 mm flat-bottom NMR tube inserted in an outer 10 mm tube filled with CCl_4.[16] In both cases, the length of the sample was constrained to 8−9 mm using custom-made Delrin or Teflon inserts, and the cylindrical symmetry axis was parallel to $\mathbf{B}_0$. Constraining of the length enabled the containment of the sample within the region of homogeneous $\mathbf{B}_0$ and, in diffusion measurements, constant field gradient.[27] Coaxial orientation of the cylindrical samples relative to $\mathbf{B}_0$ minimized shimming inhomogeneities. The homogeneity of $\mathbf{B}_0$ was adjusted typically to 3−5 Hz using the residual HDO signal from a 5 mm bulk D_2O sample; shimming was optimized again following the placement of the BCP sample. The BCP samples were packed until no significant air pockets could be seen. NMR measurements were made with at $B_0 = 9.4$ T using the same spectrometer as for the solution spectra. ^{1}H spectra were recorded using a diffusion probe equipped with either a 10 mm ^{1}H or a 5 mm ^{1}H/^{19}F resonator. ^{13}C spectra were recorded at natural abundance and without ^{1}H decoupling using the same diffusion probe with a 10 mm ^{13}C resonator. The pulsed field gradients (used in diffusion measurements) have a maximum strength 10 T m^{-1}, and the coils are actively shielded. The sample temperature (25 °C in all measurements) was calibrated using a capillary containing methanol.[29–31] NOESY spectra were acquired using a gradient-selected, phase-sensitive pulse sequence[32] with a bipolar gradient pulse applied during the mixing time. Diffusion and T_1 measurements were made as described previously.[16] Exponential apodization with 3 Hz line broadening was used for most spectra; this enabled the enhancement of the signal-to-noise ratio without significantly affecting the spectral line widths. Spectral line widths at half-height were determined by using curvilinear least-squares fitting of Lorentzian functions onto the observed line shapes. The line widths of overlapping peaks were determined using simultaneous least-squares fitting of the overlapping peaks. Further experimental details are given in the literature.[16,27]

MAS NMR Spectroscopy. MAS NMR measurements (the spinning angle 54.7° relative to $\mathbf{B}_0$) were made using a Tecmag Apollo spectrometer operating at the ^{1}H frequency 300 MHz ($B_0 = 7.05$ T). The spectrometer was equipped with a dual-channel Chemagnetics MAS probe. MAS rotors were manufactured of zirconia and had outer and inner diameters of 7 and 6 mm, respectively. The spinning speed of the sample was set using a Chemagnetics tachometer/MAS speed controller and measured precisely using the frequency separation between spinning sidebands in the NMR spectrum. Two Teflon spacers of 10 mm length were placed inside the rotor to constrain the sample. The Teflon spacers and the rotor cap were glued to the rotor using epoxy resin to prevent the ejection of the sample at large spinning speeds. The magic angle was adjusted using a KBr powder sample following the standard procedure.[33] T_1 relaxation times were measured using a conventional inversion−recovery pulse sequence.

Simulations of the Magnetic Field Maps in BCPs. The locally induced static magnetic field in the lipid and the aqueous domains of an *Im3m* BCP unit cell was simulated numerically using the surface-current technique.[34] The model used in the simulations assumed that the center of the lipid bilayer followed a Schwartz P surface geometry; the bilayer was characterized by a constant, specified thickness, and the magnetic susceptibilities of the aqueous and the bilayer domains were −9.0 and −5.0 ppm, respectively. The simulation code was written in Fortran and based on the code previously used for calculating static magnetic field maps.[35,36] The surface-current integration was carried out over a single *Im3m* unit cell with its center of symmetry placed at the origin. Because the integration was performed over a single unit cell, the distribution of the induced magnetic field $\mathbf{B}(\mathbf{r})$ in the aqueous domain was computed only for the grid points located within the "inner" aqueous subdomain (the subdomain containing the origin). The integration procedure was adapted to noncylindrical symmetry by modifying the differential surface element used for surface−current integration:[35]

$$\mathbf{B}(\mathbf{r}) = \frac{\mu_0}{4\pi}\sum_i \int\int_{S_i} \frac{\left[\frac{B_0(\Delta\chi)_i}{\mu_0}\,\mathbf{e}_i \times (\mathbf{r}-\mathbf{r}')\right]}{|\mathbf{r}-\mathbf{r}'|^3} \frac{|\mathbf{R}_i|}{(\mathbf{R}_i \cdot \mathbf{e}_i)} R_i(\varphi, z)\, \mathrm{d}\varphi\, \mathrm{d}z \quad (1)$$

where S_i is the surface of the i-th lipid−water interface; the index i refers to the inner or the outer surface of the bilayer (which is given a finite thickness expressed as a fraction of the

length of the side of the *Im*3*m* unit cell); vector $\mathbf{r}'$ spans the respective lipid−water interface; vector $\mathbf{r}$ spans the volume of the *Im*3*m* unit cell; $(\Delta\chi)_i$ is the magnetic susceptibility difference at interface i; $\mathbf{e}_i$ is a unit vector tangential to the surface of interface i and perpendicular to $\mathbf{B}_0$; $\mathbf{R}_i(\varphi, z)$ is the vector normal to the z-axis and connecting the z-axis with the point $\mathbf{r}'$; $[R_i, \varphi, z]$ are the cylindrical coordinates of vector $\mathbf{r}'$; and $|\mathbf{R}_i(\varphi, z)| = R_i(\varphi, z)$.

Typical integration parameters were as follows: 20 × 20 × 20 grid points, 4000 surface integration steps in each of the vertical (z) and the angular (φ) dimensions, and 0.02 unit cell sizes as the minimal allowed distance between a grid point and a lipid−water interface. The simulations were performed on a desktop PC (Pentium 4 CPU, 3.2 GHz, 1 GB RAM).

Results

Static Samples. ^{1}H NMR spectra from well-shimmed, nonspinning BCP samples with the cylindrical symmetry axis of the sample parallel to $\mathbf{B}_0$ were characterized by line shapes 70−100 Hz ($B_0 = 9.4$ T). A representative ^{1}H NMR spectrum of sample **2** is shown in Figure 2a. The line widths at half-height of the H_2O peak and five well-resolved lipid peaks are shown in Table 1. The different lipid line widths exhibited by the two samples are due to their slightly different compositions; this effect is discussed in the next section. In CD_3OD solution (5% myverol by weight), the respective lipid peaks exhibited a well-resolved multiplet structure (Figure 2b); the line widths of the multiplet components were approximately 0.01 ppm. The line widths of representative, well-resolved ^{13}C NMR peaks are shown in Table 2.

The T_1 values of H_2O and selected lipid peaks were measured from static sample **1** at $B_0 = 9.4$ T. T_1 values of the lipid were also measured in CD_3OD solution. The results of all T_1 measurements are shown in Table 3. The T_2 values of H_2O in static sample **1** were measured using the CPMG experiment with 180° pulse separation times $\tau = 4$, 6, 8, and 10 ms. The T_2 values were 185 ± 5 ms and were independent of τ. The values of the diffusion coefficients of H_2O and lipid in static sample **1** were 4.2×10^{-10} and 1.2×10^{-11} m^2 s^{-1}, respectively.

Two-dimensional ^{1}H NOESY spectra of sample **1** were recorded with the mixing times $\tau = 200$ and 600 ms. The spectrum recorded at $\tau = 600$ ms is shown in Figure 3a. A distinctive feature of these spectra was the elongated shape of the NOE cross-peaks between lipid peaks. Density maps of a selected well-resolved cross-peak, together with the half-height contours, are shown in Figure 3b (600 ms) and c (200 ms). A NOESY spectrum of 5% (w/w) myverol in CD_3OD was also recorded; no significant NOEs between lipid peaks were detected in this sample.

MAS Measurements. The line widths of one-dimensional ^{1}H and ^{13}C spectra were measured under MAS conditions at a series of spinning speeds ranging from 5 to 2030 Hz. At slow spinning speeds (<300 Hz), the line shapes were dominated by shimming inhomogeneities and were therefore considered uninformative. At faster spinning speeds, the line widths narrowed with increasing speed and reached an asymptotic value at approximately 500 Hz. A representative fast-spinning ^{1}H MAS spectrum is shown in Figure 2c. The line widths of the ^{1}H peaks labeled in Figure 2c are plotted in the spinning frequency range 500−2030 Hz in Figure 4. The asymptotic high-speed line width values of ^{1}H and ^{13}C peaks are shown in Tables 1 and 2, respectively.

The T_1 values of lipid and water peaks were measured under MAS conditions at $B_0 = 7.05$ T at spinning speeds 550 and 2000 Hz. The spectra were baseline-corrected using a cubic spline, and the T_1 values of the spectral peaks were determined from curvilinear least-squares fitting. The results for the selected peaks are shown in Table 3.

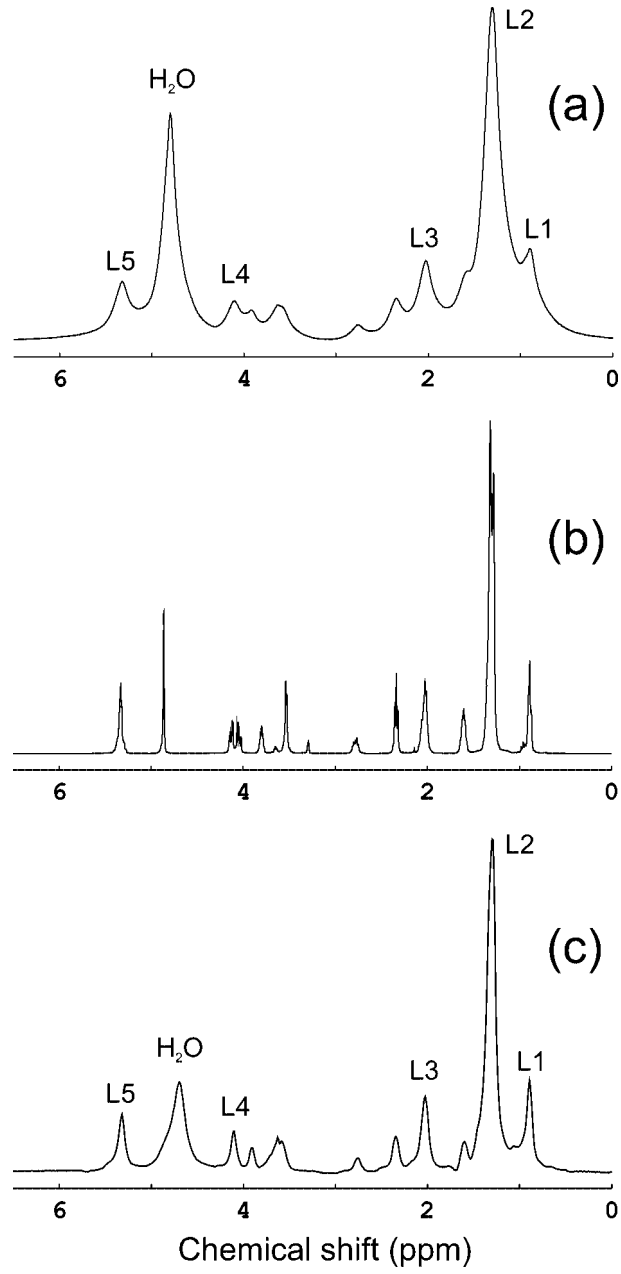

Figure 2. (a) ^{1}H NMR spectrum of myverol: H_2O BCP sample **2** (75.9:24.1% w/w) at 25 °C. The line widths of the lipid peaks labeled L1−L5 and the water peak (labeled H_2O) are shown in Table 1 and Figure 4. (b) ^{1}H NMR spectrum of 5% myverol in a CD_3OD solution. (c) MAS spectrum of sample **3** (75.2:24.8% w/w) at the spinning speed of 2030 Hz and 25 °C.

Numerical Simulations. The distribution of the local induced magnetic fields was computed numerically in four model systems placed in an external magnetic field: (i) a thin spherical shell with $\kappa = 0.083$, where κ is the ratio of the thickness of the shell to its outer radius; the material of the shell had magnetic susceptibility $\chi_{BL} = -5$ ppm; the shell contained, and was immersed in, an aqueous medium with $\chi_W = -9$ ppm;[37] (ii) a spherical shell with $\kappa = 0.33$ and the same set of magnetic susceptibilities as in (i); (iii) a thin *Im*3*m* lipid bilayer with $\kappa = 0.06$, where κ is the ratio of the thickness of the bilayer to the side length of the *Im*3*m* unit cell; the vector $\mathbf{B}_0$ was directed

TABLE 1: ^{1}H NMR Line Widths at Half-Height of Lipid and Water Peaks in Samples of Myverol:H_2O BCP at 25 °C[a]

		$\Delta\delta_{1/2}$ (ppm)			
		static samples (9.4 T)			
species	chemical shift (ppm)	sample **1**	sample **2**	MAS (sample **3**; 2000 Hz, 7.05 T)	sample **3** − sample **2** (%)
H_2O	4.8	0.10	0.20	0.18	−10
lipid					
L1	0.88	0.12	0.22	0.087	−61
L2	1.29	0.14	0.23	0.099	−56
L3	2.01	0.12	0.19	0.087	−55
L4	4.09	0.12	0.19	0.075	−60
L5	5.31	0.13	0.19	0.087	−55

[a] Samples **1**, **2**, and **3** had the lipid contents 70.0, 75.9, and 75.2% (w/w), respectively.

TABLE 2: ^{13}C NMR Line Widths at Half-Height of Lipid Peaks in Samples of Myverol:H_2O BCP at 25 °C

	$\Delta\delta_{1/2}$ (ppm)		
chemical shift (ppm)	static sample **1** (9.4 T)	MAS (sample **3**; 2000 Hz, 7.05 T)	sample **3** − sample **1** (%)
19.2	0.23	0.17	−27
76.6	0.29	0.17	−41
135.0	0.43	0.36	−16
138.0	0.33	0.24	−28
181.0	0.30	0.22	−26

along the C_4 symmetry axis of the unit cell; the bilayer had $\chi_{BL} = -5$ ppm and was surrounded by an aqueous medium with $\chi_W = -9$ ppm; (iv) an *Im*3*m* bilayer with $\kappa = 0.35$ and the same set of magnetic susceptibilities as in (iii). The field maps and distributions of B_z in the two spherical shells are shown in Figure 5. The distributions of B_z in the bilayer models were calculated separately for the lipid and the aqueous domains; the results are presented in Figure 6.

Discussion

Molecular Mobility in BCPs. BCPs represent a state of matter that is intermediate between solids and isotropic liquids. The lyotropic cubic phases have no global alignment order but possess a well-defined mesoscopic structure that is determined by the curvature of the lipid bilayer. Molecular reorientation in the BCP bilayer occurs on time scales slower than in solution but faster than in the solid state. The translational diffusion coefficient, D, of the lipid in sample **1** (1.2×10^{-11} m^2 s^{-1} at 25 °C, in the long-Δ limit) was comparable with other reported studies; for example, the lateral D of DPPC in its bilayer has been estimated as 3×10^{-11} m^2 s^{-1}.[38] This corresponds to an rms displacement, $\Delta R = (6Dt)^{1/2}$, of ~3 μm during a 200 ms NOESY mixing time; this displacement is equivalent to several hundred unit cells (using $L = 100$ Å as an estimate of the size of a cubic unit cell). An order of magnitude upper estimate of the reorientation time of lipid molecules can be obtained using the model of reorientation mediated by lateral diffusion.[13,17] As a lipid molecule performs a random walk with the diffusion coefficient D_{lat} along the bilayer, it samples the available orientations by visiting the available locations on the surface of the bilayer within the unit cell of the BCP. The corresponding rotational diffusion coefficient D_R is of the order of D_{lat}/L^2 and for a BCP unit cell can be estimated as 10^5 s^{-1}. This means that, even in the absence of flip-flop motion, a lipid molecule in a BCP samples all available orientations on the time scale of ~10^{-5} s. These estimates provide a reference point during the following discussion of NMR line shapes.

^{1}H NMR Spectroscopy of Static BCP Samples. The line widths of the lipid peaks in the static BCP samples (Figure 2a) were approximately 2 orders of magnitude greater than the respective natural line widths in a dilute solution of low viscosity (Figure 2b). The static line widths of the BCP lipid peaks shown in Table 1 tended to have similar values at a given composition. This suggests that the ^{1}H NMR line shapes in samples **1** and **2** were determined by inhomogeneous broadening rather than the natural (T_2-controlled) line width. This hypothesis was confirmed by the NOESY spectra of sample **1** (shown in Figure 3), which exhibited cross-peaks elongated along the main diagonal. Ideal absorption cross-peaks in 2D NOESY spectra have equal widths along the main and the auxiliary diagonals.[39] The elongation such as seen in Figure 3 can be explained by the presence of a distribution of local magnetic fields. The contribution to the 2D spectrum from a subensemble of dipolar-coupled proton pairs with a precession frequency ω is described as a 2D Lorentzian peak with equal line widths in the direct (ω_2) and indirect (ω_1) frequency dimensions and centered at $\omega_1 = \omega_2 = \omega$. Other subensembles, experiencing a different local magnetic field, give rise to 2D contributions that are otherwise identical but centered at a different precession frequency: $\omega_1 = \omega_2 = \omega'$. The overall 2D line shape is therefore a superposition of 2D Lorentzian peaks spread out along the main diagonal ($\omega_1 = \omega_2$) of the 2D spectrum. The eccentricity of the cross-peaks (defined as the ratio of the short axis to the long axis of the half-height contour of the cross-peak) provides a measure of the ratio of the natural line width to the inhomogeneous line width. The natural lipid line width can be estimated in sample **1** as 0.32×0.13 ppm $= 0.042$ ppm, and an extrapolation to sample **2** yields 0.32×0.20 ppm $= 0.064$ ppm. Similar inhomogeneous patterns have been observed in heteronuclear 2D spectra of BCPs,[40] as well as 2D exchange spectra of other heterogeneous systems.[22,23] The distinct feature of the NOESY spectra of BCPs is that the distribution of local environments is continuous rather than discrete, resulting in a single broad line for a given NMR peak.

Other researchers have postulated three potential contributions to inhomogeneous line shape of BCPs: (i) air bubbles or pockets present in the sample, (ii) poor shimming, and (iii) inhomogeneity of the sample itself.[19] Several of our observations demonstrate that the line widths of Tables 1 and 2 are due largely to intrinsic factors that are unrelated to sample packing or shimming. First, the line widths of the BCP peaks were reproducible to within ±10% between different BCP samples of similar composition. Second, the line widths observed in samples **1** and **2** were markedly

TABLE 3: T_1 Values of Lipid and Water ^{1}H Peaks Measured in the BCP Samples under MAS Conditions and the T_1 Values of the Lipid Peaks in CD_3OD Solution

			BCP samples		
				MAS T_1 (ms) in sample **3** (7.05 T)	
species	chemical shift (ppm)	T_1 (ms) in CD_3OD solution (9.4 T; static sample)	static T_1 (ms): sample **1**; 9.4 T	spinning at 550 Hz	spinning at 2000 Hz
H_2O	4.8	12900[a]	912	430	450
lipid					
L1	0.88	3350	821	800	770
L2	1.29	1523[b]	533	510	490
L3	2.01	1460	506	460	450
L4	4.09	1130	460	Not measured[c]	420
L5	5.31	3120	775	Not measured[c]	680

[a] Residual HDO peak. [b] The recovery curve is slightly nonexponential; the average value of T_1 is shown. [c] Not measured due to overlap of the peak of interest with a spinning sideband.

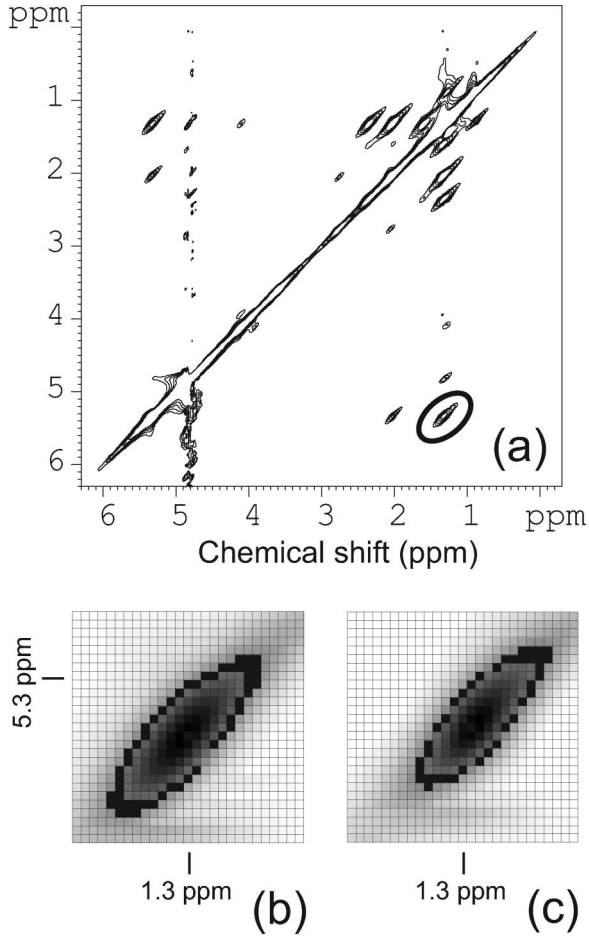

Figure 3. (a) Two-dimensional NOESY spectrum of a myverol:H_2O BCP (sample **1**, 30:70% w/w). Mixing time $\tau = 600$ ms. (b, c) The density maps of a representative cross-peak (circled in panel a) observed at (b) $\tau = 600$ ms and (c) $\tau = 200$ ms. The contours of pixels in panels b and c correspond to the half-height of the cross-peak; the eccentricity of the cross-peak is 0.32 in both cases. The size of one pixel is 3.9 Hz = 0.0098 ppm.

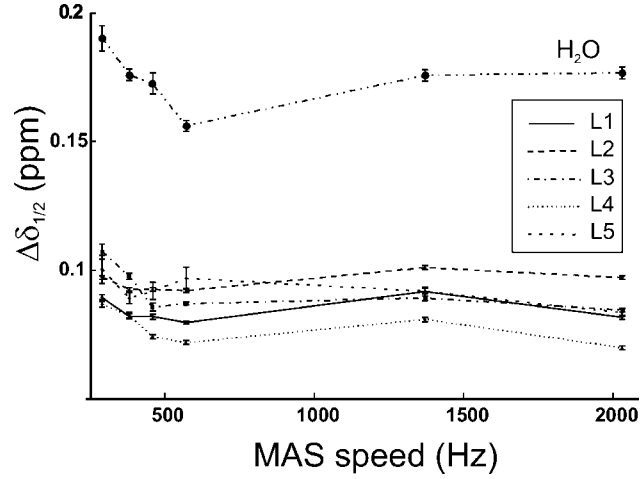

Figure 4. MAS line widths in sample **3**. The line widths of the H_2O peak (●) and the lipid peaks marked in Figure 2 (lines without symbols) are plotted as a function of the spinning speed. At the spinning speeds above 400 Hz, line widths are practically independent of the spinning speed. At low spinning speeds (<100 Hz), the line widths are determined by shimming imperfections and are considerably larger than those in the static samples **1** and **2**. The slow-spinning line widths are therefore considered uninformative. The asymptotic fast-spinning line widths correspond to the values shown in Table 1 for sample **3**.

different (as seen from Table 1); these samples had different compositions but similar apparent macroscopic viscosity and similar quality of packing. Last, the line widths observed were not significantly different between samples recorded in 5 mm Shigemi and 8 mm flat-bottom NMR tubes; the two sets of line widths would have been expected to be significantly different had the line widths been dominated by imperfect shimming. In explaining their own recent important findings,[21] Boyle-Roden et al. postulated that the BCP line broadening is due to the "end effects" caused by the geometry of the BCP sample in "conventional" setup. However, this hypothesis does not seem to explain the ability of NMR spectroscopists to obtain high-resolution spectra of "normal" samples without resorting to the use of capillaries. Indeed, spectra with resolution <5 Hz are routinely obtained from samples in conventional 5 mm Wilmad tubes without provisions for magnetic-susceptibility matching. As will be seen from the following discussion, Boyle-Roden's hypothesis also does not explain the differential line narrowing of lipid and water peaks observed in MAS measurements. We conclude that the BCP line widths reported in Tables 1 and 2 were characteristic of the lyotropic cubic phase studied and were not significantly affected by shimming or sample geometry per se.

MAS Measurements. MAS has previously been shown to result in significant narrowing of the NMR lines in BCP samples.[19] The results presented in Tables 1 and 2 also show a significant narrowing of the inhomogeneously broadened lipid peaks at spinning speeds >500 Hz. Maximal possible narrowing of the lipid peaks can be estimated based on the eccentricity of the NOESY cross-peaks: $(1 - 0.32) \times 100\% = 68\%$. The narrowing observed (55−60%) was somewhat

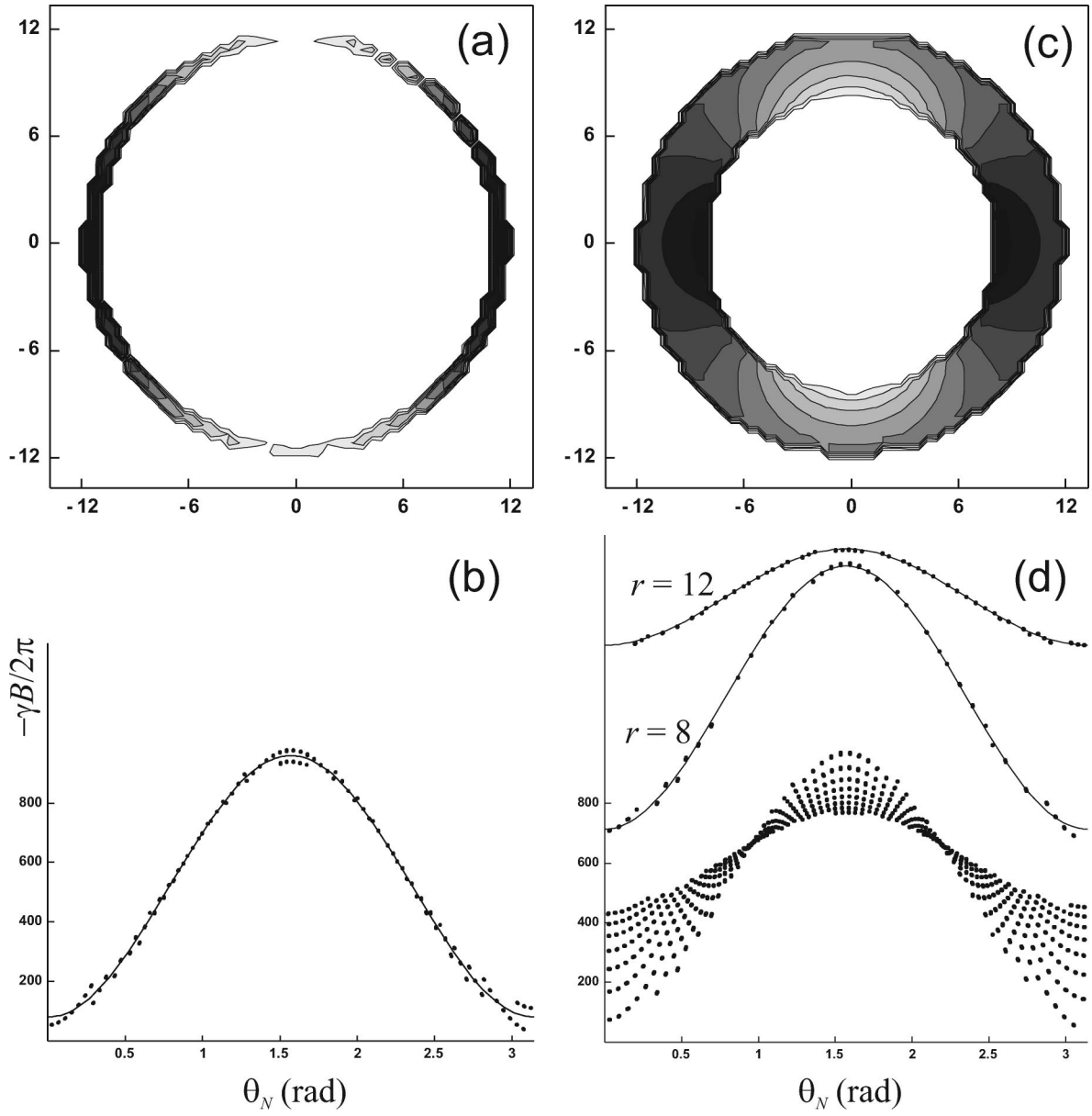

Figure 5. Simulated distributions of the induced z-component of the magnetic field, B_z, in spherical shells placed in an external magnetic field $B_0 = 5.87$ T: (a, b) relative thickness $\kappa = 0.083$; (c, d) $\kappa = 0.333$. The magnetic susceptibilities of the materials were -5 ("lipid shell") and -9 ppm ("aqueous surroundings"). Panels a and c show the field maps inside the shells. Black corresponds to the most negative values of B_z, and white corresponds to the least negative values. The field outside the shells is not shown. Panels b and d show the negative of the rotating-frame precession frequency as a function of angle θ_N (the angle between the normal to the shell's surface and the vector of the applied magnetic field $\mathbf{B}_0$). In panel d, the points corresponding to the radial positions between 8 and 8.5 mm ($r = 8$ mm) and the radial positions between 11.5 and 12 mm ($r = 12$ mm) are shown together with the respective least-squares fits to Y_{20}; these plots were vertically shifted for enhanced resolution.

smaller than this value; it was also smaller than that reported in a previous study.[19] This can be attributed to two factors: (i) Our MAS measurements were conducted at a lower temperature (25 °C) and a lower field (7.05 T) than the previous MAS study (37 °C and 11.7 T, respectively). This would have resulted in a larger natural (homogeneous) lipid line width in our measurements than in Pampel's study; (ii) Pampel and co-workers used a specially constructed MAS sample container that had a small volume, spherical shape, and susceptibility-matching inserts; this explains their ability to observe the complete MAS narrowing. This is consistent with the MAS-narrowed lipid line widths being determined by the natural T_2 values of the lipid peaks and shimming—that is, the same factors as in high-resolution NMR spectroscopy. Conversely, static lipid line widths are determined by an intrinsic inhomogeneous line width of the BCP sample. The mechanism explaining both of these hypotheses is proposed and discussed below. Importantly, the narrowing of the water peak was marginal as compared with the lipid peaks. The fact that the narrowing was limited to the lipid domain suggests that the line widths measured were determined by the mesoscopic structure of the BCP.

Effect of B_0 Magnitude. The data from samples **1** and **2** were acquired at $B_0 = 9.4$ T, while the data from sample **3** were acquired at 7.05 T. Therefore, it was important to show that the line-narrowing reported in Tables 1 and 2 was not a result of different T_2 values at the two different values of B_0. This can be seen from an analysis of the T_1 values shown in Table 3: Assuming that longitudinal relaxation of the lipid protons is due to $^1H-^1H$ dipolar coupling modulated by molecular reorientation, the relaxation rates are represented as

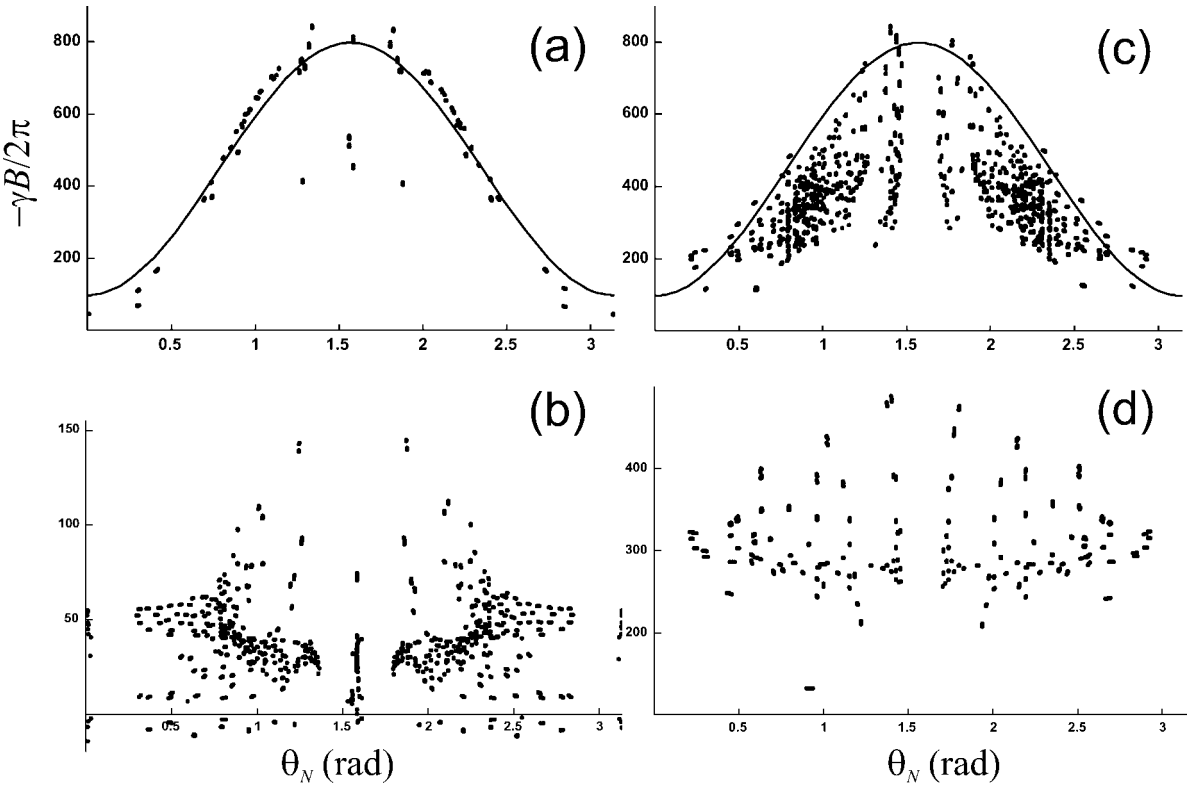

Figure 6. Same plots as Figure 5b,d but for a bilayer of *Im*3*m* geometry: (a) rotating-frame precession frequency inside the lipid bilayer, $\kappa = 0.06$; (b) inside the aqueous domain of the BCP with $\kappa = 0.06$; (c) lipid bilayer, $\kappa = 0.35$; and (d) aqueous domain of the BCP with $\kappa = 0.35$. The solid line in panel a is the least-squares fit of Y_{20} to the simulated points. The same LSF is replicated in panel c as a visual guide. The distribution of the induced B_z in the aqueous domain did not follow a simple angular dependence.

combinations of the spectral densities of molecular motion at multiples of the cyclic Larmor frequency:

$$\frac{1}{T_1} = A\sum_i \left(\frac{a_i\tau_{ci}}{1+\omega^2\tau_{ci}^2} + \frac{b_i\tau_{ci}}{1+4\omega^2\tau_{ci}^2} \right) \quad (2)$$

$$\frac{1}{T_2} = A\sum_i \left(c_i\tau_{ci} + \frac{d_i\tau_{ci}}{1+\omega^2\tau_{ci}^2} + \frac{e_i\tau_{ci}}{1+4\omega^2\tau_{ci}^2} \right) \quad (3)$$

where τ_i is the motional correlation time and $a_i - e_i$ are nonnegative constants. This result of the Redfield relaxation theory does not require for molecular reorientation to be isotropic or for it to be described by a single correlation time. The only requirement implicit in eqs 2 and 3 is that of the exponential form of motional autocorrelation functions, which is usually the case in nonsolid materials.[41]

T_1^{-1} given by eq 2 is a monotonically decreasing function of frequency. The data of Table 3 are consistent with this: The T_1 values of each proton measured were larger at 9.4 T ($\omega = 2\pi \times 400$ MHz) than at 7.05 T ($\omega = 2\pi \times 300$ MHz). Equation 3 predicts that T_2^{-1} should be a decreasing or nonincreasing function of frequency: In the limit $\tau_c \ll 1/\omega$, T_2 should be independent of the frequency; otherwise, a decrease in ω should result in an increase in T_2^{-1}. The line narrowing exhibited by sample **3** relative to the samples **1** and **2** (see Tables 1 and 2) cannot be explained by a change in the intrinsic line widths effected by a change in B_0: The effect of the decrease in B_0, if any, would have been the opposite to that observed. Therefore, we conclude that the line narrowing shown in the last columns of Tables 1 and 2 was a consequence of MAS and not the change in B_0.

Mechanism of Inhomogeneous Broadening. In the foregoing, we have shown that the inhomogeneous lipid line width originated from intrinsic factors (i.e., the two-domain structure of the BCP) rather than setup-related factors (sample packing and shimming). We now focus on the origin of this intrinsic inhomogeneity. The "traditional" mechanisms of inhomogeneous broadening include (i) internuclear dipolar interaction, (ii) anisotropy of the chemical shift tensor (for ^{13}C nuclei), and (iii) anisotropic magnetic susceptibility of the lipid. All of these mechanisms require that the time scale of molecular reorientation be comparable to the time scale of the FID (here, hundreds of milliseconds) for the inhomogeneous line shape to survive. Given that the characteristic time of molecular reorientation of the lipid could not be longer than 10^{-5} s, these mechanisms are incapable of explaining the observed NMR line inhomogeneity.

We propose a mechanism of inhomogeneous broadening that survives under fast molecular reorientation: It is well-known that the magnetic field induced in a diamagnetic object depends on its geometry and orientation relative to the applied magnetic field $\mathbf{B}_0$.[35,37,42,43] The induced diamagnetic field is uniform inside a perfect sphere and an infinitely long cylinder coaxial with the external field but not inside objects of other geometries. The BCP bilayer is a convoluted, mesoscopically structured domain that has a diamagnetic susceptibility distinct from that of the aqueous domain. Therefore, the local value of the magnetic field in a BCP can be expected to be dependent on the magnetic susceptibility difference between the lipid and the aqueous domains, the location within the unit cell, and the orientation of the unit cell with respect to $\mathbf{B}_0$. We hypothesize that the nonuniform diamagnetically induced magnetic field, determined by the geometry of the bilayer and the magnetic susceptibility difference between the lipid and the aqueous domains, serves as the origin of the inhomogeneous NMR line shapes in the BCP. This mechanism is geometrical in origin;

as shown below, it is consistent both with the inhomogeneity of NMR line shapes in the presence of fast molecular motion and with the narrowing of lipid peaks under MAS.

Numerical Simulations. To understand the effects of the magnetic susceptibility difference between the two domains of the BCP, we performed numerical simulations of the induced magnetic field in model lipid−bilayer systems. The first system simulated was a thin ($\kappa = 0.083$) spherical shell. The corresponding field map is shown in Figure 5a, and the angular dependence of the local precession frequency is shown in Figure 5b. This model system represents, for example, a large, spherical, unilamellar vesicle that is prevented from rotating. The simulated magnetic field distribution in the thin shell followed almost perfectly the angular dependence $3\cos^2\theta_N - 1$, where θ_N is the angle between $\mathbf{B}_0$ and the normal to the surface of the shell. Rapid MAS of this system should therefore result in a complete averaging of the inhomogeneous NMR line. The situation was somewhat different in the thicker ($\kappa = 0.33$) spherical shell (Figure 5c,d). There, the local magnetic field depended on the radial position within the shell as well as the angle θ_N between $\mathbf{B}_0$ and the normal to the shell. The magnetic field within a given thin spherical lamina of the shell (e.g., $r =$ 8−8.5 mm) behaved as the second-order spherical harmonic $Y_{20} = 3\cos^2\theta_N - 1$. The least-squares fits (LSF) of Y_{20} for different laminae were different. Therefore, if the shell had been filled with a continuous medium, MAS would have averaged the angular but not the radial dependence of B_z. In the case of a lipid bilayer, however, chemically distinct protons tend to reside at a given depth from the surface of the bilayer: For example, methyl end groups of the hydrocarbon tail reside deep within the bilayer and are relatively rarely exposed to the lipid−water interface. Therefore, the NMR line from a given type of lipid proton is expected to be fully narrowed by MAS.

The results of an equivalent simulation for a thin ($\kappa = 0.06$) *Im*3*m* bilayer are shown in Figure 6a,b. These results demonstrate that, inside a thin BCP bilayer, the value of the magnetic field depends only on its local orientation relative to $\mathbf{B}_0$ and it also follows the angular dependence $Y_{20} = 3\cos^2\theta_N - 1$, as above. Therefore, the local magnetic field in a thin BCP bilayer can be predicted from mapping the results of a thin spherical-shell simulation onto fragments of the BCP bilayer with the same local orientation with respect to $\mathbf{B}_0$. This result can be understood intuitively on the basis that, in the limit of an infinitely thin bilayer, the magnetic properties of a given volume element of the bilayer do not affect the magnetic field anywhere outside that volume element; that is, the induced magnetic field is a local property.

The lipid content in the BCP samples studied was 70−76%, and a thin bilayer provides a poor approximation of the actual BCP. The results of a more realistic simulation, an *Im*3*m* bilayer with $\kappa = 0.35$, are shown in Figure 6c,d. As for the thick spherical shell, the simulated field depended on the distance from the lipid−water interface as well as the local bilayer orientation. The magnetic field within a given thin lamina of the bilayer behaved approximately as $Y_{20} = 3\cos^2\theta_N - 1$, but the overall distribution was scattered. Nevertheless, as with the spherical shell, each chemically distinct type of proton is expected to reside at a given depth within the bilayer. Therefore, the broadening experienced by a given type of lipid proton is expected to follow the Y_{20} dependence and be fully narrowed by MAS. This is consistent with previous MAS studies of BCPs, where a complete averaging out of the inhomogeneity was observed.[19] The finding that the induced magnetic field within the bilayer is essentially a local property determined by the local orientation of the bilayer and the distance from the point of interest to its center is also important from the computational point of view: It justifies the use of the *Im*3*m* surface, rather than the more difficult-to-setup *Ia*3*d* surface for the numerical simulations.

Lipid Line Shape in the BCP. A diffusing lipid molecule samples several hundred BCP unit cells on the time scale of an FID, which is equivalent to sampling "all" available values of θ_N. Therefore, the magnetic susceptibility difference between lipid and aqueous domains only leads to line broadening when combined with an inhomogeneity of the sample. In BCPs, two sources of such inhomogeneity are present as follows: (i) a distribution of alignments of BCP unit cells and (ii) compositional fluctuations across the volume of the sample. The first source is always present because the periodicity of the BCP lattice does not extend to macroscopic distances and the sample does not possess a global alignment order. However, its effect on the line shape is likely to be limited because the local magnetic fields are affected primarily by the local orientation of the bilayer (see the above discussion and Figure 5). The second source can be present as a result of spatial compositional fluctuations of the sample. This provides a realistic explanation of the line broadening, especially given the recent observation of the high resolution observed in capillary BCP samples.[21] One of the distinguishing features of capillary samples, according to Boyle-Roden et al., is that these samples are "uniform and homogenous". This suggests that the compositional fluctuations across the volume of a capillary sample should be relatively low as compared to the samples prepared in the "conventional" way; this assumption is consistent with the high resolution observed in the capillary samples.

An observation that provides further support of the magnetic-susceptibility mechanism of line broadening is the relative ^{1}H line widths in samples **1** and **2**. As seen from Table 1, the static lipid line widths at $B_0 = 9.4$ T were greater in sample **2** than in sample **1**. The proposed magnetic-susceptibility mechanism explains this via the greater lipid content in sample **2**, which means that its bilayer had the greater relative thickness (regardless of the absolute size of the unit cell in the two samples). This, in turn, is consistent with greater compositional fluctuations across the sample or greater spread of induced magnetic field, leading to the relatively large inhomogeneous line width.

Water Line Shape in the BCP. Water molecules in BCPs undergo rapid exchange between free water and water that is bound to the lipid head groups.[14] In a homogeneous sample, and in the long-τ limit, the T_2 values measured from CPMG experiments should ideally be equal to the apparent T_2 estimated from the line width: $1/(\pi\,\Delta\nu_{1/2})$. This was not the case with sample **1**, which meant that the water signal was inhomogeneously broadened. As seen from Table 1, the water peak did not experience a significant line narrowing under MAS conditions. The 10% line width difference between samples **2** and **3** can be attributed to the slight difference in the composition of the samples [75.9 and 75.2% (w/w) lipid, respectively]: The lower lipid content in sample **3** corresponded to a lower molar fraction of hydration water, resulting in a longer T_2 value. This suggests that the inhomogeneous broadening of the static NMR line shape of water failed to be averaged out by MAS because the inhomogeneity did not behave as the spherical harmonic $Y_{20}(\theta_N)$. As with lipid peaks, we hypothesize that this inhomogeneous broadening was caused by the magnetic-susceptibility mechanism combined with composition fluctuations across the volume of the sample.

Practical Implications for NMR Spectroscopy of BCPs. The ^{1}H T_1values measured under MAS conditions in sample **3** were essentially equal at the two spinning speeds examined (550 Hz and 2 kHz). This suggests that the mobility of both lipid and water molecules was independent of the spinning speed within the range studied, which in turn suggests that MAS did not lead to mesoscopic reorganization of the BCP sample.

For a number of years, MAS lipid line narrowing has been used as a means of spectral resolution enhancement in NMR spectroscopy of BCPs.[19] With the recent discovery of a new line-narrowing technique,[21] the more important applications of MAS NMR to BCPs may be those in diffusion studies[20] and microimaging,[44] where MAS still provides unique advantages. MAS line narrowing is also likely to remain a source of important information concerning the microscopic organization of BCPs and could be used as a test of spatial homogeneity of the sample.

Quantitative analysis of the line broadening observed is complicated by the lack of knowledge about the intrinsic T_2 values of the lipid. A direct measurement of the homogeneous line shape of the lipid species would involve measuring T_2 values of the ^{1}H lipid peaks. This could also be used to determine whether or not residual inhomogeneities were present under MAS conditions. Unfortunately, the measurement of T_2 values of ^{1}H lipid peaks is nontrivial even in solution, due to the complicated patterns of scalar coupling in the ^{1}H NMR spectrum of myverol. Scalar couplings significantly complicate the interpretation of spin−echo or CPMG data, and the separation of T_2 relaxation and scalar-coupling effects requires customized, spin system-dependent measurements even for the relatively simple coupling patterns.[45,46] Nevertheless, if successful, this analysis would allow an unambiguous separation of the homogeneous and inhomogeneous contributions to the lipid line widths in BCP samples.

Conclusions

Myverol/water BCP samples prepared by centrifugation were studied using conventional and MAS NMR spectroscopy. In static cylindrical samples aligned with the main magnetic field, both lipid and water NMR peaks were inhomogeneously broadened. The inhomogeneous line width was strongly dependent on the composition of the BCP and significantly exceeded residual shimming line width. We demonstrate that the inhomogeneous broadening was intrinsic to the BCP and independent of instrumental factors such as shimming, the size, or the aspect ratio of the sample container. The mechanism of the broadening is the internal inhomogeneity of diamagnetically induced magnetic field, which is determined by the mesoscopic structure of the BCP and the respective diamagnetic susceptibilities of the lipid and the aqueous domains, coupled with compositional fluctuations across the volume of the sample. Both magnetic-susceptibility effect and compositional fluctuations are necessary for the inhomogeneous broadening to be present. In MAS NMR measurements, the magnetic-susceptibility effect is averaged out at spinning speeds above 500 Hz, causing the narrowing of the lipid NMR lines. The MAS-narrowed lipid line shapes are determined by the natural proton T_2 values, shimming, and the sample geometry. The NMR peak of water did not undergo MAS narrowing, which is also consistent with our proposed inhomogeneity mechanism. MAS narrowing of lipid peaks can be used as a probe of microscopic homogeneity of BCP samples. Such a test may be important for studies of the structure and dynamics of molecules that are partitioned in either the lipid or the aqueous phases of BCPs.

Acknowledgment. This work was supported by a QUT ECR Grant to K.I.M., an Invitation Fellowship from the Japan Society for the Promotion of Science to K.I.M. and K.T., and an ARC Discovery Grant to P.W.K. and Dr. J. I. Vandenberg. We acknowledge the invaluable technical assistance from Drs. Takashi Mizuno and Ryutaro Ohashi (Kyoto), Jun Fukazawa (Kyoto), and Ces De La Paz (Sydney). We thank Quest International for a gift of myverol and Dr. Mark Wellard for careful reading of the manuscript.

Abbreviations and Symbols

$\mathbf{B}_0$, the vector of the applied static magnetic field
BCP, bicontinuous cubic phase
D, diffusion coefficient
$D(H_2O)$, diffusion coefficient of water
D_L, diffusion coefficient of lipid
D_{lat}, lateral diffusion coefficient within a lipid bilayer
DPPC, dipalmitoylphosphatidylcholine
LSF, least-squares fit
MAS, magic angle spinning
NMR, nuclear magnetic resonance
NOESY, nuclear Overhauser effect NMR spectroscopy
T_1, longitudinal relaxation time
χ, magnetic susceptibility
Δ, diffusion time
$\Delta\nu_{1/2}$, line width at half-height
κ, unitless thickness of the bilayer (as a fraction of the unit cell)
θ_N, the angle between $\mathbf{B}_0$ and the normal to the bilayer

References and Notes

(1) Seddon, J. M.; Templer, R. H. Polymorphism of lipid−water systems. In *Structure and Dynamics of Membranes: From Cells to Vesicles*; Lipowsky, R., Sackmann, E., Eds.; Elsevier: Amsterdam, 1995; Vol. 1A, pp 97−160.
(2) Hyde, S. T. *Curr. Opin. Solid State Mater. Sci.* **1996**, *1*, 653–662.
(3) Shah, J. C.; Sadhale, Y.; Chilukuri, D. M. *Adv. Drug Delivery Rev.* **2001**, *47*, 229–250.
(4) Gustafsson, J.; Ljusberg-Wahren, H.; Almgren, M.; Larsson, K. *Langmuir* **1997**, *13*, 6964–6971.
(5) Okamura, E.; Nakahara, M. *J. Phys. Chem. B* **1999**, *103*, 3505–3509.
(6) Chung, H.; Kim, J.; Um, J. Y.; Kwon, I. C.; Jeong, S. Y. *Diabetologia* **2002**, *45*, 448–451.
(7) Momot, K. I.; Kuchel, P. W. *Concepts Magn. Reson.* **2003**, *19A*, 51–64.
(8) Royant, A.; Nollert, P.; Edman, K.; Neutze, R.; Landau, E. M.; Pebay-Peyroula, E.; Navarro, J. *Proc. Natl. Acad. Sci. U.S.A.* **2001**, *98*, 10131–10136.
(9) Nollert, P. *Prog. Biophys. Mol. Biol.* **2005**, *88*, 339–357.
(10) Siegel, D. P. *Biophys. J.* **2006**, *91*, 608–618.
(11) Shearman, G. C.; Ces, O.; Templer, R. H.; Seddon, J. M. *J. Phys.: Condens. Matter* **2006**, *18*, S1105–S1124.
(12) Anderson, D. M.; Wennerström, H. *J. Phys. Chem.* **1990**, *94*, 8683–8694.
(13) Håkansson, P.; Persson, L.; Westlund, P. O. *J. Chem. Phys.* **2002**, *117*, 8634–8643.
(14) Eriksson, P. O.; Lindblom, G. *Biophys. J.* **1993**, *64*, 129–136.
(15) Lindblom, G.; Orädd, G. *Prog. Nucl. Magn. Reson. Spectrosc.* **1994**, *26*, 483–515.
(16) Momot, K. I.; Kuchel, P. W.; Whittaker, D. *Langmuir* **2004**, *20*, 2660–2666.
(17) Althoff, G.; Frezzato, D.; Vilfan, M.; Stauch, O.; Schubert, R.; Vilfan, I.; Moro, G. J.; Kothe, G. *J. Phys. Chem. B* **2002**, *106*, 5506–5516.
(18) Szutkowski, K.; Stilbs, P.; Jurga, S. *J. Phys. Chem. C* **2007**, *111*, 15613–15619.
(19) Pampel, A.; Strandberg, E.; Lindblom, G.; Volke, F. *Chem. Phys. Lett.* **1998**, *287*, 468–474.
(20) Pampel, A.; Karger, J.; Michel, D. *Chem. Phys. Lett.* **2003**, *379*, 555–561.
(21) Boyle-Roden, E.; Hoefer, N.; Dey, K. K.; Grandinetti, P. J.; Caffrey, M. *J. Magn. Reson.* **2007**, *189*, 13–19.
(22) Moudrakovski, I. L.; Ratcliffe, C. I.; Ripmeester, J. A. *Appl. Magn. Reson.* **1995**, *8*, 385–399.
(23) Alam, T. M.; Brow, R. K. *J. Non-Cryst. Solids* **1998**, *223*, 1–20.

(24) Robyr, P.; Gan, Z. *J. Magn. Reson.* **1998**, *131*, 254–260.
(25) Tycko, R., Ed. *Nuclear Magnetic Resonance Probes of Molecular Dynamics (Understanding Chemical Reactivity)*; Springer: New York, 2003.
(26) Clogston, J.; Rathman, J.; Tomasko, D.; Walker, H.; Caffrey, M. *Chem. Phys. Lipids* **2000**, *107*, 191–220.
(27) Momot, K. I.; Kuchel, P. W.; Chapman, B. E.; Deo, P.; Whittaker, D. *Langmuir* **2003**, *19*, 2088–2095.
(28) Momot, K. I.; Kuchel, P. W. *J. Magn. Reson.* **2004**, *169*, 92–101.
(29) Ammann, C.; Meier, P.; Merbach, A. E. *J. Magn. Reson.* **1982**, *46*, 319–321.
(30) Momot, K. I.; Walker, F. A. *J. Phys. Chem. A* **1997**, *101*, 9207–9216.
(31) Ma, J. H.; Guo, C.; Tang, Y. L.; Chen, L.; Bahadur, P.; Liu, H. Z. *J. Phys. Chem. B* **2007**, *111*, 5155–5161.
(32) Wagner, R.; Berger, S. *J. Magn. Reson. A* **1996**, *123*, 119–121.
(33) Duer, M. *Introduction to Solid-State NMR Spectroscopy*; Blackwell Publishing: Oxford, United Kingdom, 2004.
(34) Purcell, E. M. *Berkeley Physics Course: v. 2. Electricity and Magnetism*; McGraw-Hill: New York, 1965.
(35) Momot, K. I.; Binesh, N.; Kohlmann, O.; Johnson, C. S. *J. Magn. Reson.* **2000**, *142*, 348–357.
(36) Momot, K. I.; Johnson, C. S. *J. Chem. Phys.* **2001**, *115*, 3992–4002.
(37) Doty, F. D.; Entzminger, G.; Yang, Y. A. *Concepts Magn. Reson.* **1998**, *10*, 133–156.
(38) Essmann, U.; Berkowitz, M. L. *Biophys. J.* **1999**, *76*, 2081–2089.
(39) Ernst, R. R.; Bodenhausen, G.; Wokaun, A. *Principles of Nuclear Magnetic Resonance in One and Two Dimensions*; Clarendon Press: Oxford, 1987.
(40) Larkin, T.; Momot, K. I.; Kuchel, P. W. *NMR Studies of Diffusion in Bicontinuous Cubic Phases*; ANZMAG Conference: Murramarang, NSW, 2006.
(41) Abragam, A. *Principles of Nuclear Magnetism*; Clarendon Press: Oxford, 1961.
(42) Kuchel, P. W.; Chapman, B. E.; Bubb, W. A.; Hansen, P. E.; Durrant, C. J.; Hertzberg, M. P. *Concepts Magn. Reson.* **2003**, *18A*, 56–71.
(43) Durrant, C. J.; Hertzberg, M. P.; Kuchel, P. W. *Concepts Magn. Reson. Part A* **2003**, *18A*, 72–95.
(44) Pampel, A.; Zick, K.; Glauner, H.; Engelke, F. *J. Am. Chem. Soc.* **2004**, *126*, 9534–9535.
(45) Takegoshi, K.; Ogura, K.; Hikichi, K. *J. Magn. Reson.* **1989**, *84*, 611–615.
(46) Larkin, T. J. NMR studies of solute dynamics in a bicontinuous cubic phase. B.Sc. (Honours) Thesis, University of Sydney, 2005.

JP8006415